Three-Dimensional Structure and Dynamics of a de Novo Designed, Amphiphilic, Metallo-Porphyrin-Binding Protein Maquette at Soft Interfaces by Molecular Dynamics Simulations

5 **AUTHORS**, INCLUDING:

Joseph Strzalka
Argonne National Laboratory
92 PUBLICATIONS   **1,729** CITATIONS

SEE PROFILE

Andrey Tronin
University of Pennsylvania
24 PUBLICATIONS   **247** CITATIONS

SEE PROFILE

Kent Blasie
University of Pennsylvania
147 PUBLICATIONS   **3,729** CITATIONS

SEE PROFILE

Three-Dimensional Structure and Dynamics of a de Novo Designed, Amphiphilic, Metallo-Porphyrin-Binding Protein Maquette at Soft Interfaces by Molecular Dynamics Simulations

Hongling Zou, Joseph Strzalka, Ting Xu, Andrey Tronin, and J. Kent Blasie*

Department of Chemistry, University of Pennsylvania, Philadelphia, Pennsylvania 19104

Received: October 9, 2006; In Final Form: December 11, 2006

The three-dimensional structure and dynamics of de novo designed, amphiphilic four-helix bundle peptides (or "maquettes"), capable of binding metallo-porphyrin cofactors at selected locations along the length of the core of the bundle, are investigated via molecular dynamics simulations. The rapid evolution of the initial design to stable three-dimensional structures in the absence (apo-form) and presence (holo-form) of bound cofactors is described for the maquettes at two different soft interfaces between polar and nonpolar media. This comparison of the apo- versus holo-forms allows the investigation of the effects of cofactor incorporation on the structure of the four-helix bundle. The simulation results are in qualitative agreement with available experimental data describing the structures at lower resolution and limited dimension.

Introduction

There is already substantial interest in utilization of the cofactors that impart functionality in biological systems in artificial peptide-based macromolecular assemblies to develop biomolecular materials for novel electronic and photonic device applications.[1−5] For example, amphiphilic four-helix bundle peptides, designated "maquettes",[6] have been designed de novo for such purposes to incorporate both biological and nonbiological cofactors, the latter exhibiting extraordinary electron transfer and nonlinear optical properties.[7] The amphiphilicity directs their vectorial orientation in Langmuir monolayers at soft interfaces between polar and nonpolar media.[3,8,9] This property enables the formation of large ordered monolayer ensembles of the maquettes on a macroscopic scale, including on surfaces of solid inorganic substrates,[10,11] thereby facilitating fabrication of a functional material.

Gaining knowledge of the detailed three-dimensional (3-D) structure of these maquettes is essential to providing sufficient insight into the structure−function relationships of such systems necessary to manipulate (i.e., control) the functionality of one or more cofactors within the artificial peptide. In particular, it is important to achieve accurate structural information on the holo-form of the amphiphilic maquettes (i.e., with incorporated cofactors), especially in the neighborhood of the cofactors, within the vectorially oriented monolayer ensembles. Unfortunately, the usual methods for 3-D structure determination have not been successful, even for water-soluble maquettes. In fact, only one X-ray crystal structure of a water-soluble antiparallel four-helix bundle maquette (designated as BB), capable of binding metallo-porphyrin cofactors with high specificity, has been determined,[12] but only for the less relevant apo-form (i.e., without the cofactors). NMR spectroscopy was not successful in determining the structure of the apo-form of this water-soluble maquette in isotropic aqueous solution due to the dynamic nature of the interface between dihelices.[13] With no 3-D structural information available to date for the holo-form of any of the
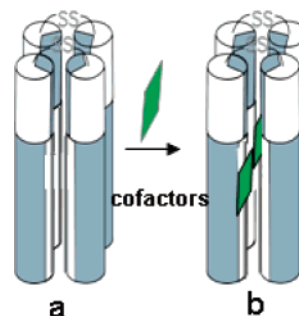

Figure 1. (a) Rigid solid-cylinder model for an amphiphilic protein maquette. (b) The peptide bundle is capable of binding cofactors at the interior site of the bundle through bis-histidyl ligation, which suggests two binding sites in the bundle of the F6H20 variant. The cylinder exterior is in white (hydrophobic surface) and gray (hydrophilic surface). The solid slabs represent the approximately planar metallo-porphyrin cofactors.

more simple water-soluble maquettes, one would expect that obtaining this information for amphiphilic four-helix bundle maquettes would be even more problematic by analogy to their biological membrane protein counterparts. In any event, such information as obtained for membrane proteins using the detergent-solubilized maquette in 3-D crystals or isotropic solutions might not be of any relevance to that for amphiphilic four-helix bundle maquettes vectorially oriented within the highly anisotropic environment of a soft interface between polar and nonpolar media. This absence of 3-D structural information has led to very simple models for the maquettes based on rigid solid-cylinder representations for the helices, their association to form four-helix bundles assumed to be directed by their amphipathic design, and solid slabs representing the approximately planar metallo-porphyrin cofactors, as shown in Figure 1.[8,14]

Classical molecular dynamics (MD) simulations have the capability to provide the otherwise unavailable atomic-resolution 3-D structure of such maquettes in such highly anisotropic environments. They have achieved notable success in providing the structure and dynamics as essential to the properties of such

* Author to whom correspondence should be addressed. E-mail: jkblasie@sas.upenn.edu.

complex systems, including proteins in isotropic aqueous solution,[15,16] fully hydrated anisotropic lipid bilayers,[17,18] and membrane proteins incorporated into such lipid bilayers.[19,20] In addition, MD simulation has the advantage of readily investigating maquette structure and dynamics in different environments that may not be easily accessed in the experiment, for example, at an ideal interface where the stability of its design can be tested as well as in laboratory-accessible interfacial environments, thus allowing predictions for and comparison with experiments. As a "benchmark" test of the MD methods and force field for the system of interest, we performed simulations on the four-helix bundle of BB, extracted from the available crystal structure and placed in an isotropic water environment, for ~10ns. The isolated bundle structure of BB was thereby found to be very stable and well preserved in bulk water.[21]

We utilize MD simulations to investigate the structure and dynamics of a new family of amphiphilic α-helical bundle peptide maquettes that have been recently designed and characterized.[8,9,22] One of these maquettes, designated "AP0", binds both biological and nonbiological cofactors containing a metallo-porphyrin with high specificity at selected locations along the length of the bundle's interior.[3,5,8] These amphiphilic bundles have been successfully inserted vectorially into the soft interfaces between polar and nonpolar media as provided by a phospholipid monolayer at the water−air interface. MD simulations were performed on the apo-form of AP0 and a holo-form with the biological Fe−porphyrin cofactors, at two different interfaces. An ideal water−octane interface was used to address the stability of the initial model structures to the anisotropy of the interface. In this case, the hydrophilic and hydrophobic domains of the bundle, oriented with its long axis perpendicular to the interface, would be anticipated to interact only with their respective water and octane environments, in the absence of any interactions with neighboring bundles and/or applied external forces. We found that the model structures for both forms are unstable, evolving rapidly to substantially different structures that subsequently stabilize over the ~10 ns trajectories, while maintaining the time-averaged orientation of the bundle's long axis perpendicular to the interface. Importantly, the structure of the holo-form of the AP0 maquette is dramatically affected by incorporation of the cofactor and aspects of its chemical structure.

However, it is extremely difficult to realize any definitive experimental results for the water−octane system. To date, only very simple amphiphiles (e.g., long-chain alcohols) have been studied at a water−alkane interface.[23] Conversely, complex amphiphiles, with limited solubility in either polar or nonpolar media such as these amphiphilic four-helix bundle AP0 maquettes, are much more easily studied in Langmuir monolayers at the water−air interface with the control of lateral surface pressure.[8] The helices associate to form four-helix bundles with their long axis oriented perpendicular to the interface only at higher surface pressures, corresponding to minimal average areas per helix in the plane of the interface. In this situation, the hydrophobic domain of the bundle is presumably stabilized by favorable nonpolar interactions with those domains of neighboring bundles. For a more direct comparison with the experiment, we therefore also performed ensemble simulations for both the apo- and the holo-forms of AP0 at a water−air interface. These results were in much better agreement with the available experimental X-ray scattering data than the initial model structures. Thus, these simulations provide the first 3-D atomic-level view of the structure of the apo- and holo-forms of the AP0 maquette bundles at soft interfaces as well as the in-

trabundle dynamics within different regions of the maquette. They also demonstrate that a more definitive comparison with experiment would be provided by neutron reflectivity employing the deuteration of selected residues along the length of the peptide.

Materials and Methods

Model System. *Peptide Construction.* We selected the F6H20 variant[5] of the prototypical amphiphilic four-helix bundle peptide maquette AP0 for simulation (i.e., the mutation H6H20 → F6H20 was made). This variant of AP0 was chosen to place the Fe−porphyrin cofactor closer to the interface between the hydrophilic and the hydrophobic domains of the maquette where it could function as an acceptor for electron transfer across the interface. For convenience, we will simply refer to this as "AP0" subsequently. The helices of both the apo- and the holo-forms of AP0 dimerize via disulfide bond formation between the cysteine residues at the C-terminus, while two dihelices associate to form a four-helix bundle.[8] Two Fe−protoporphyrin IX (FePPIX) cofactors can bind to the four-helix bundle via bis-histidyl axial ligation with the H20 residues on each helix to saturate the available binding sites. This particular holo-form will simply be referred to as "holo-AP0" hereafter.

For the simulations, the peptides were initially constructed as ideal right-handed α-helices using INSIGHTII (Accelrys Software Inc.). The SCADS algorithm[24] was applied to apo-AP0 to provide a minimal energy four-helix bundle structure. For holo-AP0, one FePPIX was positioned within each dihelix through bis-histidyl ligation, which is energetically favorable.[25] The interhelix rotation (rotation of the helices about their long axis) and separation for holo-AP0 were adjusted to satisfy the geometrical requirement of bis-histidyl ligation. The relative orientations of the two FePPIX cofactors for holo-AP0 were determined by energy minimization for the system, including the peptide, cofactors, and water molecules within hydrogen-bonding distance of the cofactors, for a number of discrete rotations of the cofactors about the normal to the porphyrin plane (i.e., about the axial ligation Fe−N bond).

Single Bundle at the Water−Octane Interface (for Apo-AP0 and Holo-AP0). n-Octane (C_8H_{18}) was chosen for the nonpolar medium because it is a relatively simple liquid that forms a stable interface with H_2O at room temperature.[26]

The pre-equilibrated C_8H_{18} slab was placed on top of the pre-equilibrated H_2O slab to form the MD cell, and the amphiphilic peptide bundle was inserted at the interface between the two slabs with the interface between the hydrophilic and the hydrophobic domains of the bundle aligned with that between the slabs. The solvent molecules that overlapped with atoms of the peptide or cofactors were removed, as were those in the core region of the peptide bundle. The lateral dimensions (52 × 52 Å^2) of the MD cell were set such that the four-helix bundle was well separated from the periodic images in the plane of the interface. Similarly, the height of each solvent slab was made large enough (extending beyond each end of the peptide bundle another 40 Å) such that the bundle and the interface were well separated from the periodic images in the *z*-direction normal to the interface. Thus, the MD cell dimensions were chosen large enough to ensure the isolation of both the amphiphilic four-helix bundle and the interface while employing periodic boundary conditions to model an intrinsically two-dimensional monolayer system in the simulations. This requirement remained valid throughout the entire simulation. Figure 2 shows the initial setup for apo- and holo-forms of AP0 at the water−octane interface.
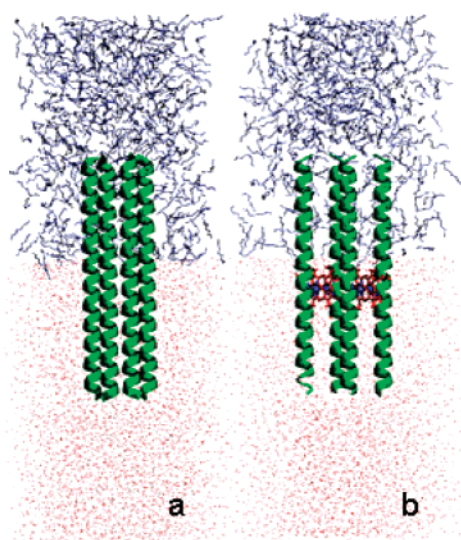
Structure and Dynamics of a Protein Maquette

J. Phys. Chem. B, Vol. 111, No. 7, 2007 **1825**

Figure 2. Side view of the initial configurations for simulations of the isolated four-helix AP0 at the water−octane interface: (a) apo-AP0 and (b) holo-AP0. The helices are shown in ribbon representation, and the solvent is shown in wire-frame representation with hydrogen atoms omitted for clarity. Octane is shown in silver and, water is shown in red. In part b, FePPIX cofactors are shown in red wire-frame representation.

Ensemble of Bundles at the Water−Air Interface (for Apo-AP0 and Holo-AP0). The equilibrated isolated peptide bundles for the apo- and holo-forms of AP0 that had evolved to a stable quaternary structure at the water−octane interface were extracted and duplicated providing nine replicas for each case. The nine bundles were uniformly distributed onto a square grid (81 × 81 Å^2) in the plane of the interface. Each bundle was rotated by 90° about the z-axis normal to the interface with respect to its neighbors to achieve a more "random" arrangement thereby providing not exactly the same environment for each peptide bundle. A pre-equilibrated H_2O slab was used to solvate the hydrophilic domains of the peptide bundles. The bundles were closely packed, and the lateral dimension of the simulation cell was chosen small enough to mimic a highly compressed "monolayer" of AP0 at the interface with an average area/helix of ~180 Å^2. The height of the MD cell was made more than twice that of the physical extent of the system along the z-direction perpendicular to the interface to avoid interference from its periodic images in that direction. The initial configurations for the apo- and holo-forms of AP0 are shown in Figure 3 for the ensemble simulation system at the water−air interface. Our choice of the equilibrated isolated bundle structure from the water−octane system as the initial configuration for the ensemble simulation for each form of AP0 was necessary to attain such a small average area/helix for the holo-form. The significance of this choice will be presented in the Discussion section.

Altogether, each ensemble simulation system contains ~62 000 atoms.

Equilibration and Dynamics. For the peptide/water/octane system, 50 ps of solvent equilibration was performed with peptide coordinates constrained to eliminate the tension between different components. The energy of the peptide bundle was subsequently minimized for 1000 steps. The system was then heated over 100 ps to a final temperature at 300 K. Dynamics trajectories were then generated for the simulation systems under constant NPT conditions over 5 ns. For holo-AP0, the peptide was constrained to ideal α-helices by applying a restraint potential with an energy barrier of 50 kcal/mol on the backbone
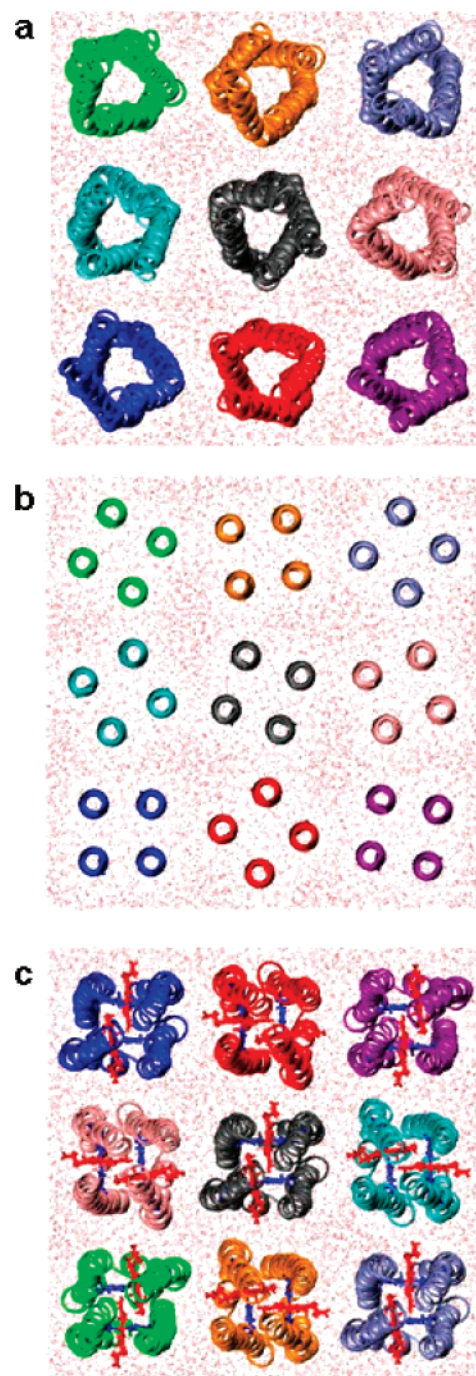

Figure 3. Top view of the initial configurations for the ensemble simulation at the water−air interface. Both the (a) apo-AP0 and the (c) holo-AP0 systems were constructed using the pre-equilibrated peptide bundles taken from the previous simulation at the water−octane interface. Considering the near circular symmetry of the cross-section of the pre-equilibrated bundles, each bundle was rotated by 90° about the z-axis normal to the interface with respect to its neighbors in parts a and c. To investigate whether the choice of the initial configuration prejudices the results, we also studied the system with straight uncoiled helices as the initial configuration, as shown in part b, briefly described as follows. In part b, each bundle being square in cross-section was rotated by 40° about the z-axis normal to the interface with respect to its neighbors to achieve a more "random" arrangement of the bundles; the simulation cell was chosen small enough to provide an average area per helix of ~180 Å^2. The helices are shown in ribbon representation with each helical bundle colored differently for clarity. Water is shown in red wire-frame representation. In part c, FePPIX cofactors are shown in red wire-frame representation as are the H20 residues highlighted in blue.

1826 *J. Phys. Chem. B, Vol. 111, No. 7, 2007*

Zou et al.

dihedrals during the energy minimization and heating stages. This restraint was used to create space for the FePPIX cofactors without introducing local distortions to the structure initially. The constraint was then released for the following 5 ns of the NPT dynamics trajectory.

For the ensemble simulation system, the initial procedures consisting of solvent equilibration, energy minimization, and heating were also performed. NPT dynamics trajectories over 3 ns were then generated.

All of the simulations were carried out using the NAMD2 package[27] and the CHARMM22 all-atom force field.[28] The TIP3P model[29] was used for water molecules. The parameters used for octane were those recommended by MacKerell et al.[28] for methyl and methylene groups. The force field for six-coordinate planar FePPIX was implemented within CHARMM22 with specification of the dihedral about Fe$-$His ($N_{His}-C1_{His}-C2_{His}-Fe$) as recommended by Autenrieth.[30] Constant temperature was controlled by Langevin dynamics, and the pressure was maintained at 1 atm using the Nosé$-$Hoover Langevin piston method.[31] Periodic boundary conditions were employed in all cell dimensions, and the particle-mesh Ewald (PME) method[32] was used for full evaluation of the electrostatic interactions. Nonbonded interactions were calculated with a cutoff distance of 10 Å, and a switching function was employed to relax the van der Waals potential to zero over a distance of 2 Å. The SHAKE algorithm[33] was used to constrain all bonds between hydrogen atoms and heavy atoms with a tolerance of 10^{-8} Å. A time step of 2 fs was used for bonded and nonbonded interactions, and full electrostatic forces were evaluated every other time step. We note that the overall MD simulation approach employed here, including the simulation algorithm and force field, are currently widely utilized for membrane proteins embedded within hydrated lipid bilayers, as entirely analogous to the systems of interest herein.

Data for analysis were taken from the last 1 ns of the trajectories, over which the area/four-helix bundle in the plane of the interface and the conformation of the four-helix bundle peptide were stable.

Experimental Section. The methods of data collection and analysis for X-ray reflectivity, grazing-incidence X-ray diffraction, and UV$-$vis absorption spectroscopy experiments have been reported elsewhere.[11]

Results and Discussion

Structure of the Isolated AP0 Peptide and Its Stability at the Water$-$Octane Interface. *Apo-Peptide Structure.* Examination of instantaneous configurations over the course of the MD trajectory indicates that the initial configuration for the isolated four-helix bundle of the apo-form is unstable at the interface and evolves rapidly to a stable, left-handed coiled-coil structure. This is demonstrated objectively by several measures. First, the root-mean-squared deviation (rmsd) for the backbone atoms with respect to the initial configuration summed over all residues evolves over the first 500 ps of the trajectory to a value of 5.50 ± 0.35 Å, which is subsequently stable for the remainder of the 6 ns trajectory as shown in Figure 4a. Second, the crossing angle between neighboring helices is typically used to describe coiled-coil structures (measured as the angle between the principal axes of two neighboring helices; this angle is approximately twice the pitch angle of the major helix of the coiled coil).[34,35] The crossing angle for each pair of neighboring helices in the bundle is also seen to rapidly evolve similarly for each pair over the first 500 ps of the trajectory from zero to $19° \pm 2°$, which is then also stable for
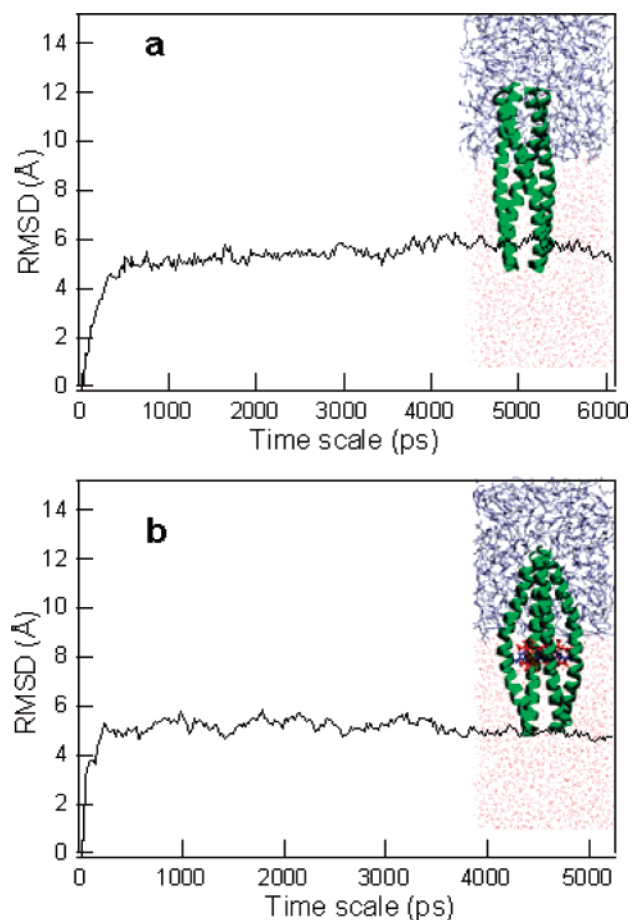

Figure 4. Evolution of the rmsd of backbone atoms with respect to the initial configuration calculated from the simulations of (a) apo-AP0 and (b) holo-AP0 at the water$-$octane interface. Inset: Side view of the instantaneous configuration representing the equilibrated structure for each form. The color code is the same as in Figure 2.

the remainder of the 6 ns trajectory as shown in Figure 5a. Third, the φ and ψ backbone dihedral angles define the nature of the secondary structure present in peptides and proteins. A Ramachandran plot of the time-averaged $\varphi-\psi$ pairs of all residues, except the N-terminal capping residues and C-terminal Gly loop residues, indicates that a majority of residues remain within the allowed region for a α-helical conformation over the entire trajectory (Figure 6, circles).

The resulting coiled-coil structural motif arises from the de novo design of the apo-form, which was based on the heptad repeat, denoted as abcdef in the seven-residue pattern. For the hydrophilic domain, residues at the "a" and "d" positions were chosen to be nonpolar to form a hydrophobic core for the bundle in an aqueous medium. Upon formation of the coiled-coil structure, the side chains in the hydrophobic core of the bundle were driven to tight packing, thus maximizing the van der Waals interactions, as shown in Figure 7. During the entire trajectory, fewer than four water molecules penetrate the interior of bundle. These water molecules were attracted by the polar H20 residue of each helix. This suggests that better packing could be achieved for the apo-form by mutating the H20 histidine to a less polar residue. However the H20 residue was designed to be in the interior of the bundle to form a metal ligation site for the holo-form of the four-helix bundle maquette. For the hydrophobic domain of the peptide, the explanation is the opposite; namely, the tighter packing of the uncharged polar residues forms a hydrophilic core for the bundle in a nonpolar medium stabilized by van der Waals and charge-compensating
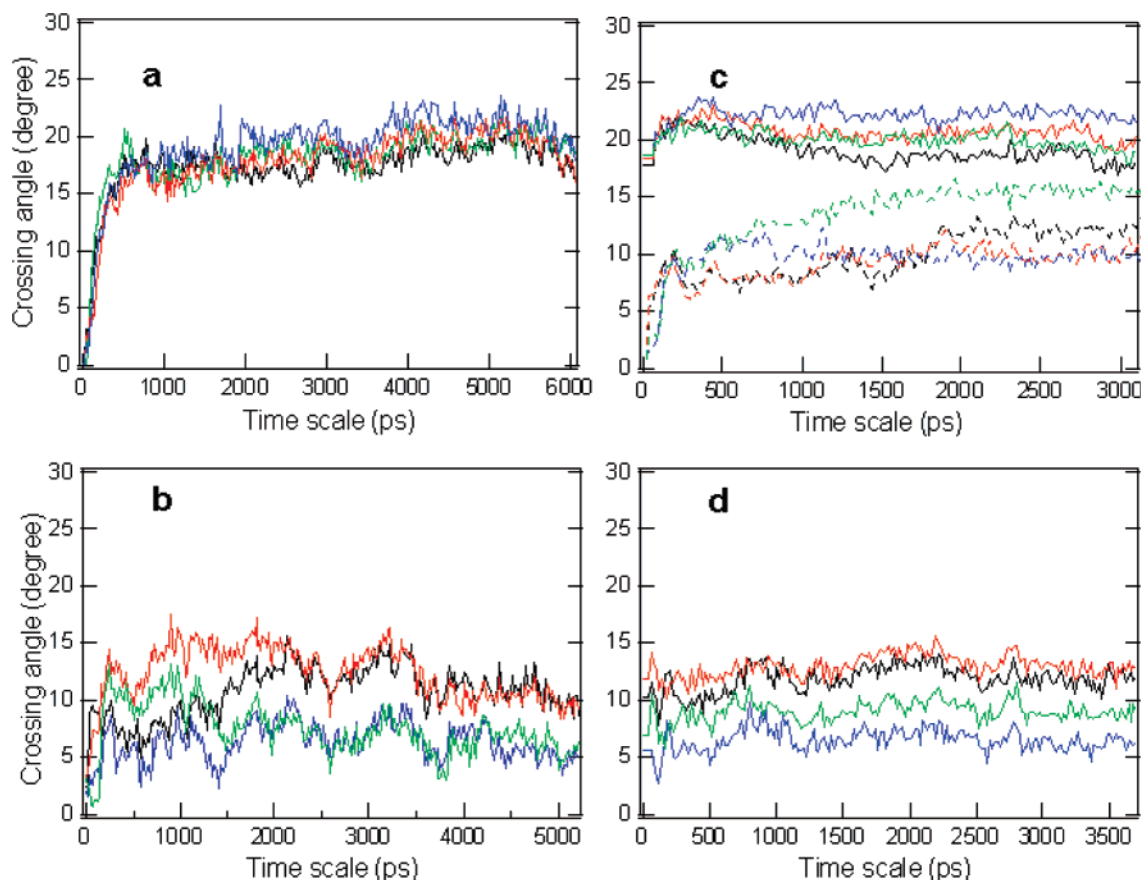
Structure and Dynamics of a Protein Maquette

J. Phys. Chem. B, Vol. 111, No. 7, 2007 **1827**

Figure 5. Evolution of the crossing angle between neighboring helices within the peptide bundle: (a) calculated from the apo-AP0 isolated bundle simulation at the water−octane interface and (c, in solid lines) continued in the ensemble simulation at the water−air interface; (b) calculated from the holo-AP0 isolated bundle simulation at the water−octane interface and (d) continued in the ensemble simulation at the water−air interface. The crossing angle calculated from the ensemble simulation of the apo-AP0 starting from straight uncoiled-coil helices is included in part c (in dashed lines) to compare with the result of ensemble simulation of the apo-AP0 starting from the pre-equilibrated structure as illustrated above. Intra-dihelical crossing angles, defined as the crossing angle measured between the two neighboring helices within either dihelix, are in black and red. Inter-dihelical crossing angles, defined as the crossing angle measured between the neighboring helices from different dihelices, are in blue and green.
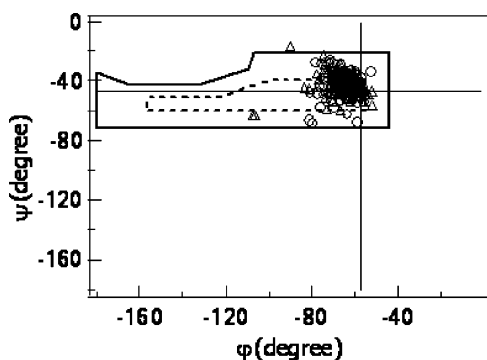

Figure 6. Ramachandran plot for residues 2−42 in all of the helices of the four-helix bundle AP0 at the water−octane interface. The backbone conformation angles φ and ψ are calculated as averages over the last 1 ns of the simulation for both apo- (circles) and holo-forms (triangle) of AP0. The straight lines indicate the "ideal" values of φ and ψ for right-handed α-helical structures. The dashed perimeter corresponds to the "core" region representing the most favorable combinations of $\varphi-\psi$ values for right-handed α-helical conformations, and the solid perimeter shows the "allowed" region.

interactions, the latter including hydrogen-bonding among Gln residues, as also shown in Figure 7. The closely packed and coiled-coil structure results in a narrow distribution of interhelix separations of 11−12 Å with a fluctuation of only ±0.4 Å along the bundle. The only residues that deviated slightly from ideal $\varphi-\psi$ pairs are residues H20 and E21, consistent with the above,

namely, the placement of the polar H20 residue in the otherwise nonpolar interior of the hydrophilic domain. These deviations, however, did not occur on the same residues in all four helices of the apo-form, which suggests only a small local distortion of the helical structure. There was also no indication of any backbone distortion for residues in the region between the hydrophilic and hydrophobic domains of the amphiphilic bundle. Thus, the design tightly coupling the hydrophobic domain and the hydrophilic domain to form a stable, amphiphilic four-helix bundle peptide with a coiled-coil structure throughout appears successful.

Holo-Peptide Structure. Examination of instantaneous configurations over the course of the MD trajectory indicates that the initial configuration for the isolated four-helix bundle of the holo-form is also unstable at the interface but evolves much less rapidly to a spindlelike structure, which is definitely not a uniform coiled coil over its length. This is also demonstrated objectively by several measures. First, like the apo-form, the rmsd for the backbone atoms with respect to the initial configuration summed over all residues evolves over the first 500 ps of the trajectory from zero to a value of 5.11 ± 0.28 Å, which appears subsequently stable for the remainder of the 6 ns trajectory as shown in Figure 4b. However, the crossing angle for each pair of neighboring helices in the bundle evolves much less rapidly and differently for each pair over the first 3−4 ns of the trajectory. While the crossing angles for each pair are
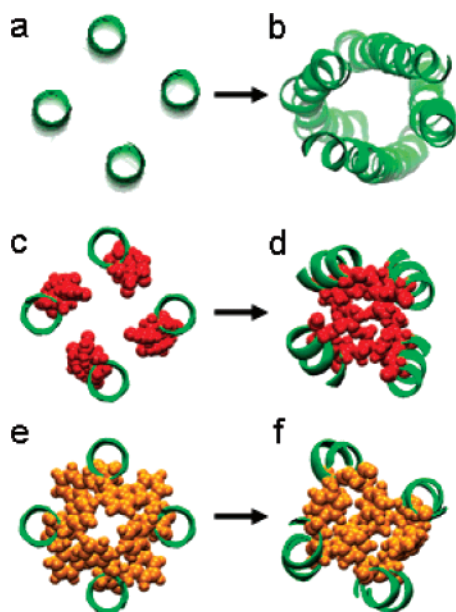
Figure 7. Instantaneous configurations of the isolated four-helix bundle apo-AP0 (a, c, and e) initially and (b, d, and f) after 5 ns of simulation at the water−octane interface viewed from the C-terminus along the bundle long axis. The helices are shown in a ribbon representation, and the interior residues are shown in a space-filling representation. Complete sequences of the peptides are shown in parts a and b to illustrate the overall change in peptide structure. (c and d) One heptad is shown from the hydrophobic domain to demonstrate the packing of the interior polar residue Gln in red. (e and f) One heptad is shown from the hydrophilic domain to demonstrate the packing of the interior nonpolar residues in orange.

Figure 8. Instantaneous configurations of the isolated four-helix bundle holo-AP0 (a) initially and (b−e) after 5 ns of simulation at the water−octane interface viewed from the C-terminus along the bundle long axis. Complete sequences of the peptides are shown in parts a and b to illustrate the overall change in peptide structure. The helices are shown in a ribbon representation, and FePPIX is shown in a wire-frame representation. One heptad is shown from (c) the hydrophilic domain, (e) the hydrophobic domain, and (d) in the middle of bundle where the FePPIX cofactors are bound, respectively, to demonstrate the interior packing within each domain and the change of interhelix separation along the bundle. In parts c−e, the helices are shown in a ribbon representation, while the interior residues are shown in a space-filling representation. (c) Interior residues in the hydrophilic domain are shown in orange, (e) while Gln and Ala in the hydrophobic domain are shown in red and purple, respectively. (d) FePPIX cofactors are in yellow, and His is in blue.

subsequently stable for the remainder of the 6 ns trajectory as shown in Figure 5b, the intra-dihelical crossing angle stabilizes to a value of $11° \pm 2°$ while the inter-dihelical crossing angle stabilizes to a smaller value of $6° \pm 2°$. Both of these crossing-angle measures for the holo-form are much smaller than that for typical coiled-coil structures like the apo-form. Nevertheless, the Ramachandran plot of the time-averaged $\varphi-\psi$ pairs of all residues (also shown in Figure 6), except the N-terminal capping residues and C-terminal Gly loop residues, indicates that a majority of the residues remain within the allowed region for an α-helical conformation over the entire trajectory.

The resulting spindlelike structure for the bundle is seen to arise from a nonuniform expansion of the interhelix separation over the length of the bundle. The interhelix separation expanded within the cross-section of the central portion of the bundle necessary to accommodate intercalation of the FePPIX cofactors at that location, relative to the apo-form. This expansion causes the interhelix separation within the central portion of the bundle to become 3−4 Å larger than the interhelix separation at the ends of the bundle (10−11 Å), which thereby results in a much larger fluctuation (± 1.4 Å) of the interhelix separation along the bundle compared to that of the apo-form (± 0.4 Å). The interhelix separation contracted toward the ends of the bundle to retain a tight packing of the helices within the bundle's cross-section analogous to the apo-form. This contraction toward the ends of the bundle was more pronounced within the hydrophilic domain (interhelix separation of ∼10 Å) than that in the hydrophobic domain (interhelix separation of ∼11 Å), as shown in Figure 8. The propionic groups of both cofactors extended to the surface of the bundle exposed to the solvent, while the methyl and vinyl groups project into the interior of the bundle (Figure 8b). In the two regions immediately adjacent to the cofactors along the length of the interior of the bundle, a cavity
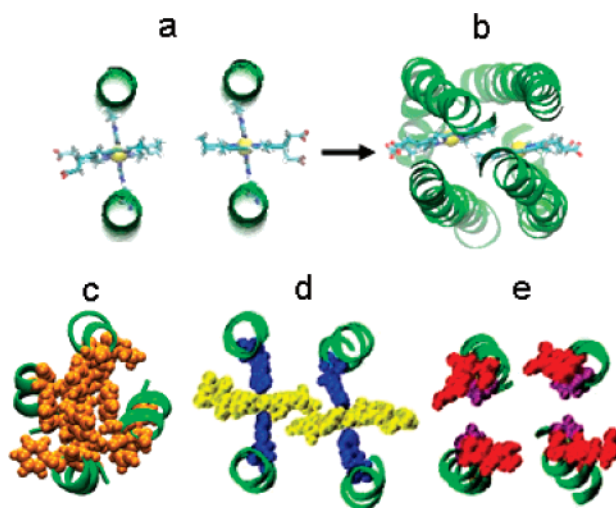
results from cofactor incorporation due to the inability of the helices to achieve close-packed interhelix separations over short distances, as opposed to toward the more distant ends of the bundle. The residues in the interior of the hydrophilic domain are generally larger in size (e.g., Phe) than the residues in the interior of the hydrophobic domain (e.g., Ala and Gln). Thus, the cavity in the hydrophilic domain is more effectively filled than that in the hydrophobic domain, resulting in four octane molecules entering the latter over the course of the MD trajectory. Fewer than four water molecules penetrate the interior of the bundle in the hydrophilic domain. These water molecules were attracted by the polar H20 residue of each helix as in the case of apo-AP0. The above explains the nonuniform distribution of interhelix separations along the length of the bundle for the holo-form, resulting in an average separation greater than that for the apo-form. The only residues that deviated slightly from ideal $\varphi-\psi$ pairs were some of the mutated residues (F6) and neighboring residues. In the hydrophilic domain, nonpolar residues F6 should occur in the "a" or "d" positions of the heptad repeat to form the nonpolar core. However, in the initial configuration of the simulation for the holo-form, F6 could not be positioned completely in the interior when H20 was placed in the interior to have the appropriate geometry for axial ligation of the iron atom of the cofactor. During the dynamics, rotation of some of the F6 residues into the interior of the bundle could induce some small local distortion of the backbone. This result suggests that H6 should have been mutated to a residue more polar than phenylalanine to remove the metal ligation site at the 6-position as desired for this variant of AP0.

Amphiphilicity of the Peptide Maquettes. Figure 9 shows the variation in the orientation of the isolated peptide bundle at the water−octane interface over the course of the MD trajectory
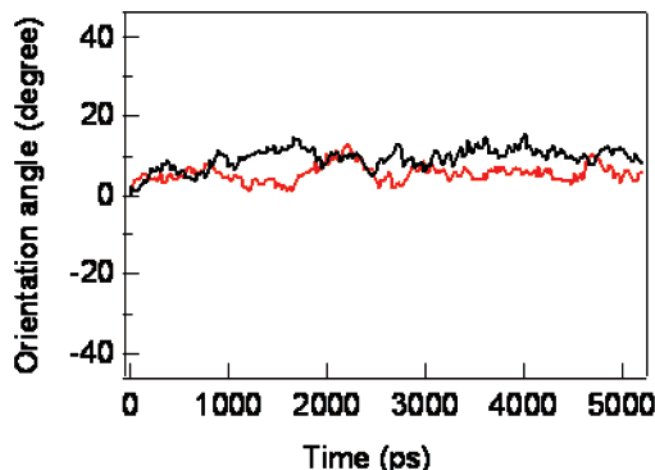
Structure and Dynamics of a Protein Maquette

J. Phys. Chem. B, Vol. 111, No. 7, 2007 **1829**

Figure 9. Evolution of orientation of the peptide bundle long axis for apo-AP0 (black) and holo-AP0 (red) at the water−octane interfaces. A value of 0° corresponds to the bundle long axis perpendicular to the plane of the interface.

for both the apo- and the holo-forms. This orientation is defined as the angle between the normal vector to the plane of interface (i.e., the *z*-axis of the simulation coordinate frame) and the long principal axis of the peptide bundle. For both the apo- and the holo-forms, the four-helix bundles were initially placed with their long axis perpendicular to the interface. The orientation angles for both the apo- and the holo-forms are stable through the 6 ns trajectory at the values of 5.4° ± 2.3° and 8.2° ± 2.8°, respectively, as shown in Figure 9. Although the orientation of the bundle long axis fluctuates substantially about the normal to the plane of the interface over the course of the trajectory for both forms, the average orientation remains close to normal to the plane. We note that for these simulations of the isolated bundles the area of the MD cell in the plane of the interface is ∼2400 Å^2, which corresponds to a square with a ∼70 Å diagonal comparable to the length of the bundle. That is sufficient to allow the bundles to tilt and eventually lie with their long axis in the plane of the interface, should that be favorable energetically. However, the water−octane interface appears to provide a favorable environment for solvation of both domains of the amphiphilic four-helix bundle peptide, suggesting that it could be vectorially oriented at such soft interfaces even at a very large interfacial area per bundle. Furthermore, incorporation of FePPIX cofactors to create the holo-form does not significantly affect the orientation of the amphiphilic AP0 at the water−octane interface. This important result suggests that the amphiphilic four-helix bundle peptide positions itself at the interface between polar and nonpolar media, consistent with its design, namely, according to the polarity of the exterior residues for each domain.

Structure and Dynamics of the AP0 Peptide Ensemble at the Water−Air Interface. The MD simulations described above suggest that the water−octane interface stabilizes the amphiphilic AP0 maquette's structure by providing favorable interactions with the environment for each domain. The simulation system demonstrates that the maquettes should orient vectorially with their long axis perpendicular to the interface, even at relatively large average areas per helix in the plane of the interface, in the absence of any interactions with neighboring bundles and without applying external forces. However, as noted in the Introduction, it is extremely difficult to realize any definitive experimental results for the water−octane system. Instead, these amphiphilic four-helix bundle AP0 maquettes are much more easily studied in Langmuir monolayers at the water−

air interface with the control of lateral surface pressure. However, the helices associate to form four-helix bundles with their long axes oriented perpendicular to the interface only at higher surface pressures, corresponding to minimal average areas per helix in the plane of the interface. In this situation, the hydrophobic domain of the bundle is presumably stabilized by favorable nonpolar interactions with those domains of neighboring bundles. The MD simulations described above at relatively large average areas per helix in the plane of the water−octane interface are consistent with this conclusion. For example, the absence of the octane in the otherwise identical initial configuration results in the dissociation of the four-helix bundle structure in the hydrophobic domain over the course of the trajectory to allow the helices to lie on the water surface (as consistent with their amphipathic design), while only the hydrophilic domain remains stable as a four-helix bundle with its long axis remaining approximately perpendicular to the interface. Thus, simulation of an ensemble of the amphiphilic four-helix bundle maquettes vectorially oriented at the water−air interface at near minimal average areas per helix in the plane of the interface would be much closer to the attainable experimental situation.

Apo- and Holo-Peptide Structures. Upon insertion of the pre-equilibrated bundles into the ensemble systems, further evolution of bundle structure over the subsequent time course of the ensemble trajectories for both the apo- and the holo-form was observed. This is demonstrated by both the length of bundle and the crossing angle of neighboring helices.

In Figure 10, we show that the length of the bundle evolves from its initial value over the first ∼2 ns of the trajectory for each form of the peptide in the isolated bundle simulations and is then stable over the remainder of the trajectories. However, in the subsequent ensemble simulations, the length of the bundle exhibits a further decrease of ∼4 Å over the first 500 ps and then is stable for the rest of the trajectory. The length of the bundle for both forms of the peptide stabilized to a value of 54.5 ± 0.2 Å in spite of the local structure change induced by intercalation of cofactors for the holo-form. The range of crossing angles for both forms of the peptide does not change significantly, namely, 17−22° for the apo-form and 5−12° for the holo-form (Figures 5c and 5d). However, the crossing angles between each pair of neighboring helices, measured within and between dihelices, now differ more greatly in the ensemble simulation. We note that the environment about the bundle axis provided by the neighboring bundles in ensemble simulation is less isotropic than that for the isolated bundle in the water−octane system. These results suggest that the structure of the peptide bundle will indeed be affected by the interface; therefore, the ensemble simulation is necessary to provide important results directly relevant to experiments.

We also investigated ensemble simulations on the apo-form starting from an initial configuration of straight uncoiled helices, at an average area per helix in the plane of the interface of ∼180 Å^2 (Figure 3b), namely, the same area as the ensemble simulation for the apo-form starting from a pre-equilibrated initial configuration. The bundle structure rapidly evolved over the first 500 ps of the trajectory to that of a coiled coil with a crossing angle of ∼6−10°, which subsequently continued to slowly increase, reaching ∼10−15° by the end of the 3 ns trajectory (Figure 5c). Thus, it seems that starting from either straight or pre-equilibrated configurations might result in a coiled-coil structure with comparable crossing angles given sufficient time. This suggests that the ensemble simulations are not seriously prejudiced by the utilization of the pre-equilibrated
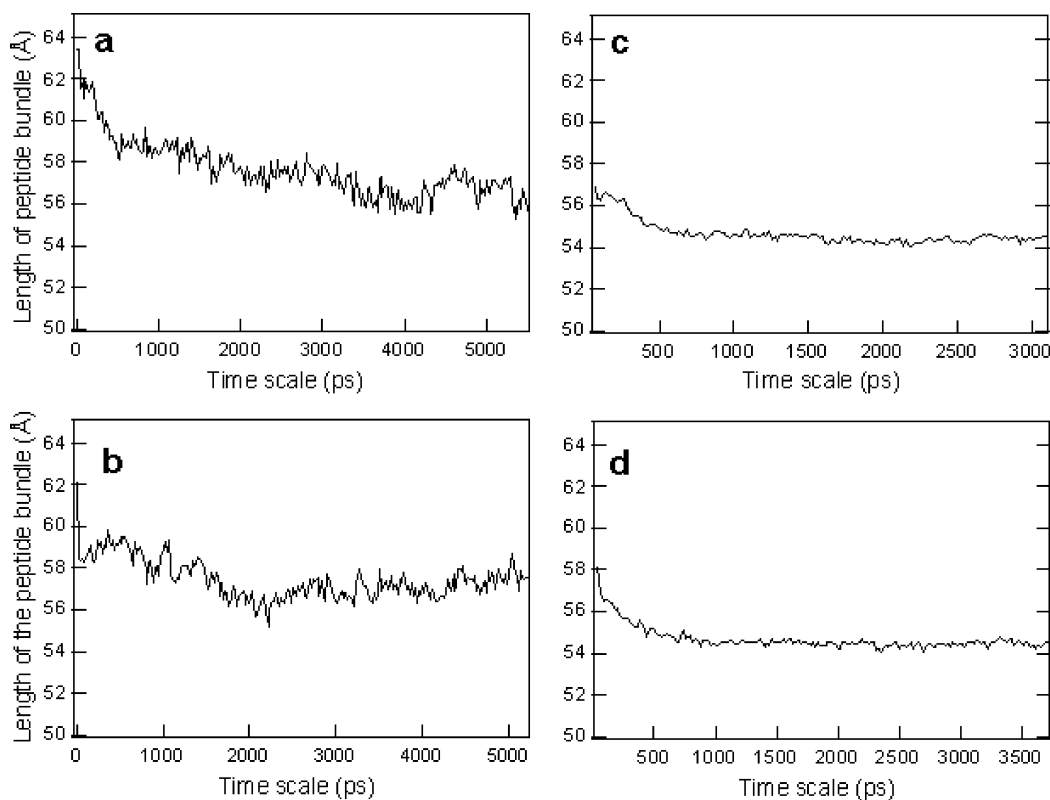
Figure 10. Evolution of the length of the peptide bundle: (a) calculated from the apo-AP0 isolated bundle simulation at the water−octane interface and (c) continued in the ensemble simulation at the water−air interface; (b) calculated from the holo-AP0 isolated bundle simulation at the water−octane interface and (d) continued in the ensemble simulation at the water−air interface. The length of the bundle is measured as the distance between the center of mass for the first residue to the center of mass for the last residue projected onto the bundle long axis.

initial configuration, taken from the isolated bundle simulations at the water−octane interface, for both the apo- and the holo-forms.

For the holo-form, only the initial configuration taken from the end of the isolated bundle simulation at the water−octane interface could be utilized to provide an average area per helix in the plane of the interface of ∼180 $Å^2$, sufficiently small for the ensemble simulation. The utilization of straight uncoiled helices with intercalated cofactors in the initial configuration for the holo-form results in a much larger, and therefore unsuitable, average area per helix in the plane of the interface (as demonstrated in Figure 2b).

Bundle and Cofactor Orientation Distributions. Figure 11 shows the time-averaged orientation distribution of the normal to the plane of the cofactor's porphyrin ring for the holo-form. The width of this distribution, when fit with a single Gaussian function, is seen to be substantially broader (∼12° full width at half-maximum) compared to that of the long axis of the four-helix bundle (∼7°). A better fit is provided by a bimodal distribution represented by two Gaussian functions whose means differ by ∼10°. This suggests that the relative mean orientations of the two cofactors dominate the width of their average orientational distribution instead of the cofactor's motions (as allowed by the conformational flexibility of the two H20 residues of the dihelix that link the cofactor's Fe atom (via axial ligation to the π-N atom of each H20 residue) to the backbone of each helix). Thus, while the cofactors' motions may be restricted by the intercalation of the relatively large porphyrin ring into the interior of the four-helix bundle, the utilization of the electronic absorption and emission transitions of the metallo-porphyrin cofactor, which are polarized in the plane of the ring, will provide an experimentally determined width for the orientation distribution of the two cofactors relative to the plane
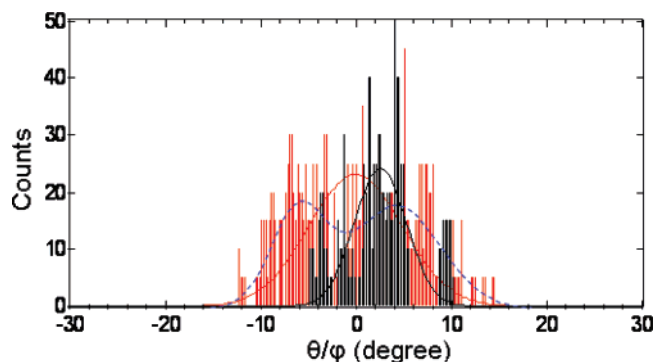

Figure 11. Orientation distributions of the FePPIX cofactors (θ, red bars) and the peptide bundles (φ, black bars) for holo-AP0 from the ensemble simulations at the water−air interface. A value of 0° for the orientation angle θ of the cofactor corresponds to the normal to the plane of the cofactor's porphyrin ring parallel to the plane of the interface. The orientation angle of the bundle long axis φ is defined in Figure 9. The red and black curves are obtained by fitting one Gaussian function to the orientation distributions of θ and φ, respectively. A better fit of the orientation distribution of θ was provided by two Gaussian functions (in the blue dashed curve). However, one overall distribution is likely to represent the orientation distribution of the two cofactors relative to the plane of the interface determined experimentally.

of the interface[36] that is likely to be larger than that of the orientation distribution of the four-helix bundle itself.

Monolayer Electron Density Profiles Derived from X-ray Reflectivity. The time-averaged electron density profile for the apo- and holo-forms of the AP0 peptide can be derived from the X-ray reflectivity data from Langmuir monolayers of the respective peptides. The electron density profile arises from the average structure of the monolayer projected parallel to the plane of the water−air interface onto the normal to the interface. It
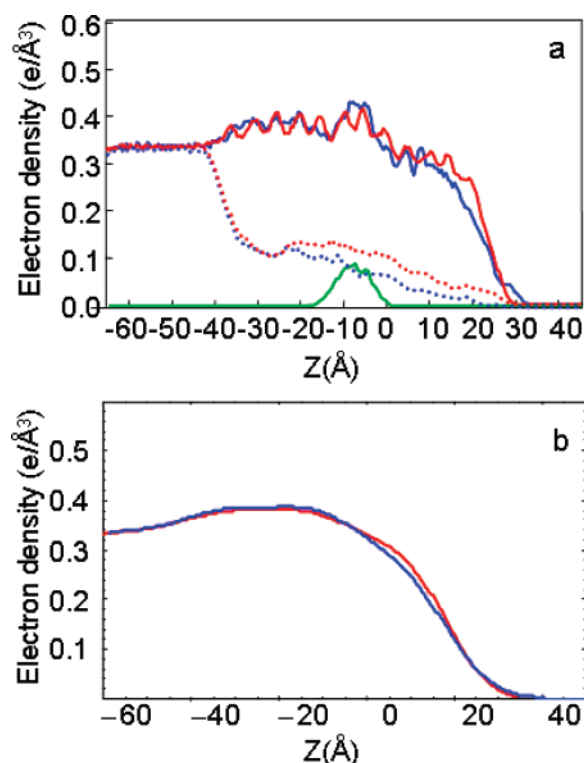
Structure and Dynamics of a Protein Maquette

J. Phys. Chem. B, Vol. 111, No. 7, 2007 **1831**

Figure 12. (a) Electron density profiles predicted from the ensemble simulation systems for apo- (red) and holo-AP0 (blue) at the water−air interface. The electron densities were calculated averaged on all of the components in the system over the final 1 ns of the MD trajectory (solid lines). The origin of the z-axis is arbitrary and was originally chosen to be approximately at the interface. The profiles for water are shown in dotted lines. The profile for the FePPIX cofactors is in green. (b) For comparison with the results from the X-ray reflectivity experiment, the profiles of the entire system for apo- (magenta) and holo-AP0 (blue) have been convoluted with a Gaussian function whose width corresponds to a spatial resolution more comparable to the experiment, namely at ∼10 Å.

can provide the extension of the amphiphilic bundle normal to the plane of the interface as well as variations in the average local density of the bundle along its length when the bundle long axis is oriented normal to the plane of the interface at higher lateral surface pressures. Details in the latter local density variations depend on the spatial resolution inherent in the calculated profile.[8,37]

Comparisons of the electron density profiles for the apo- and holo-forms of the AP0 peptide from the ensemble simulation systems at the water−air interface, averaged over the last nanosecond of their respective trajectories, are shown in Figure 12a. These time-averaged profiles indicate that the lengths of both the apo- and the holo-forms of the four-helix bundle peptide normal to the plane of the interface are nearly identical to within ∼0.5 Å and, importantly, 8−9 Å shorter than that of ∼63 Å for their respective initial configurations at the water−octane interface consisting of straight, untilted, and uncoiled helices, as shown in Figure 10. The length of the peptide bundle for both the apo- and the holo-forms of AP0 and the similarity of this length between the two forms are fully consistent with the available experimental monolayer electron density profiles. The effectively atomic resolution in the average profiles from the ensemble simulation exhibit variations along the length of the bundle that differ in detail for the apo- versus holo-forms, especially in the vicinity of the cofactors present in the holo-form. Unfortunately, given the nature of these profiles (i.e., the averaging associated with the projection), such differences arise from the superposition of effects due to the presence of the

cofactors and their induced changes in the bundle structure. These effects remain inseparable, even at such high spatial resolution. Furthermore, these differences are almost completely obscured when these profiles from the ensemble simulation are convoluted with the experimental spatial resolution of ∼10 Å, as shown in Figure 12b.

Average Intrabundle Structure from Grazing-Incidence X-ray Diffraction. Grazing-incidence X-ray diffraction (GIXD) from Langmuir monolayers of the apo- and the holo-forms of the AP0 peptide compressed to higher lateral surface pressures arises from the intrabundle structure cylindrically averaged about the normal to the interface and exhibits negligible effects of interbundle interference due to glasslike, in-plane positional ordering of the bundles.[3,11] It can provide the number of helices in the bundle, the symmetry of their arrangement in the cross-section of the bundle, the interhelix separation averaged over the length of the bundle, and the nature of the coiled-coil structure averaged over the length of the bundle if present.[3] The corresponding GIXD expected from the monolayer ensemble simulations can therefore be calculated as the cylindrically averaged structure factor for the central bundle in the nine-bundle ensemble according to

$$|S(Q_{xy},Q_z)|^2 = |\sum_j Z_j\, e^{i\mathbf{Q}\mathbf{R}_j}|^2$$

where Z_j is the atomic number of the jth atom, the photon momentum transfer vector $\mathbf{Q}$ has been resolved in components parallel (Q_{xy}) and perpendicular (Q_z) to the interface, $\mathbf{R}_j$ is the vector position of the jth atom in the MD cell, and the sum extends over all atoms in the MD cell, which is then time-averaged over the last nanosecond of the trajectory.

Figure 13a shows the Q_{xy} dependence of the diffraction maximum arising from interhelix interference effects within the four-helix bundle predicted from simulations. It suggests that the shape of the diffraction maximum should not change as its position shifts to lower Q_{xy} by ∼10% upon intercalation of two FePPIX cofactors per bundle, converting the apo- to the holo-form of AP0. This shift corresponds to an increase in the average interhelix separation within the bundle of ∼1 Å in terms of the average separation between the nearest-neighbor helices within the cross-section of the bundle. Furthermore, the layer-line modulation of the Q_z dependence of this diffraction maximum arising from the coiled-coil quaternary structure of the apo-AP0 bundle predicts coiled-coil parameters for the pitch of the major helix $P \approx 157$ Å and a pitch angle $\alpha \approx 13.5°$ and that this modulation of the Q_z dependence should essentially vanish upon conversion to the holo-form (Figure 13b). The available experimental GIXD data (not shown) are in qualitative agreement with these two predictions from the ensemble simulations. Namely, for stoichiometries of less than two FePPIX cofactors per four-helix bundle, the average interhelix separation is increased, and the average coiled-coil structure is diminished relative to the apo-form.

Intrabundle Structural Detail Available via Neutron Reflectivity and MD Simulation. As described above, the monolayer electron density profiles provided by X-ray reflectivity provide little information concerning the internal structure of the four-helix bundle, including differences between the apo- and the holo-forms, due in part to their relatively low spatial resolution. Even if the resolution were dramatically improved, the total electron density profile for the ensemble cannot provide much detail because of the average nature of the projection and the comparable electron densities of the various amino-acid residues. However, the internal structure of the bundle would be largely
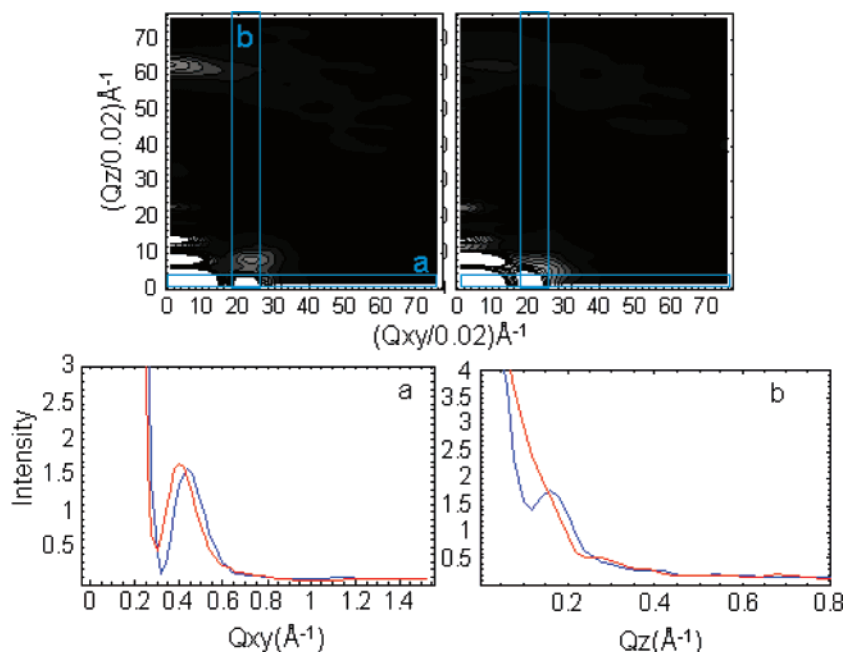
Figure 13. GIXD predicted from the ensemble simulations of the AP0 peptide at the water−air interface. Upper panels: Contour plots of the modulus square of the cylindrically averaged structure factor $S(Q_{xy}, Q_z)$ for apo- (left) and holo-AP0 (right) with averages over all nine bundles at one instantaneous configuration. Lower left panel: Integrations over Q_z of the region indicated by "a" in the upper contour plots to give the Q_{xy} dependence of the maximum in the structure factor modulus dominated by interhelix interference in the neighborhood of $Q_z \approx 0$ Å^{-1}. Lower right panel: Integrations over Q_{xy} of the region indicated by "b" in the upper contour plots to give the Q_z dependence of the structure factor modulus in the region dominated by interhelix interference within the bundle. Color code: apo-AP0, blue; holo-AP0, red.

TABLE 1: Mean Positions (MPs) and Half-Widths (HWs) of the Individual Residues of AP0 along the Length of the Bundle Obtained from Ensemble Simulation at the Water−Air Interface[a]

residue	MP of the apo-form	HW of the apo-form	MP of the holo-form	HW of the holo-form	$\Delta(MP_{apo} - MP_{holo})$
L42	24.15	6.11	24.00	6.43	+0.15
L40	23.82	4.87	22.09	5.71	+1.73
L37	19.80	4.12	19.00	4.41	+0.80
L33	14.83	4.74	14.10	4.12	+0.73
L30	10.43	3.99	10.19	3.78	+0.24
L27	6.11	3.81	5.45	3.63	+0.66
R23	−0.17	4.52	−1.23	4.19	+1.06
E22	−0.31	4.19	−1.39	3.54	+1.08
E21	−3.02	4.09	−3.29	3.76	+0.27
FePPIX	N/A	N/A	−3.60	5.55	N/A
H20	−4.14	3.70	−4.14	3.30	0
L19	−4.96	3.83	−6.48	3.43	+1.52
K18	−7.73	4.53	−8.96	4.17	+1.59
L17	−9.15	4.03	−9.67	3.44	+0.52
E15	−10.56	3.92	−12.75	3.41	+2.19
F13	−14.44	3.79	−14.96	3.35	+0.52
F6	−24.76	4.15	−25.66	3.81	+0.90
E1	−31.61	4.67	−31.41	3.93	−0.20

[a] The mean position z_0 and half-width σ of each residue were obtained by fitting a Gaussian function $A \exp[-(z - z_0)^2/\sigma^2]$ to the time-averaged electron density profile of each individual residue. To facilitate comparison, the offset along the length of the bundle between the two systems was adjusted to superimpose the mean positions of H20 from two systems. The values are given in units of ångstroms.

determined if the time-averaged positions and widths characterizing the distribution of individual residues along the length of the bundle were known from experiment. For example, Table 1 shows the mean position and half-width of the individual residue distributions for both the apo- and the holo-forms of AP0, as obtained by fitting a Gaussian function to the time-averaged electron density profile of each residue in the ensemble simulations. Although the overall length of the four-helix bundle peptide is not affected by cofactor incorporation into the bundle

(i.e., calculated by MP(L42)-MP(E1)), the mean positions of individual residues along the length of the bundle are seen to differ by as little as 0.15 Å to as much as 2.2 Å between the apo- and the holo-forms. This range of differences in mean positions of the residues is thereby indicative of significant differences in the separations of particular pairs of residues along the long axis of the bundle between the apo- and the holo-forms. These altered separations of residue pairs are a direct measure of the structural changes in the bundle necessary to accommodate the cofactors. Furthermore, the widths of the individual residue distributions are systematically smaller for the holo-form compared to the apo-form over almost the entire length of the bundle, except near the end of the hydrophobic domain where they are larger for the last six residues. This suggests that upon incorporation of the cofactors the mean positions of the residues along the length of the bundle, particularly within the hydrophilic domain containing the cofactor binding sites, are better defined for the holo-form. Recently, it has been shown that specular neutron reflectivity, coupled with the deuteration of selected amino acid residues at one or two sites per measurement, is capable of providing the mean position of an individual residue within the monolayer profile, i.e., along the long axis of the bundle, with an accuracy of ±0.5 Å.[38] Although the monolayer electron density profiles of the two systems remain quite similar, the simulations show that the differences in the mean positions of a number of residues within the monolayer profile upon converting the apo- to the holo-form well exceed the accuracy of the neutron experiment. Thus, neutron reflectivity could provide the level of structural detail necessary for a more definitive comparison of the ensemble simulations with experiment.

Conclusion

The MD simulations described have provided the first 3-D atomic-level view of an amphiphilic four-helix bundle maquette, designed to form a coiled coil and insert vectorially at a soft

Structure and Dynamics of a Protein Maquette

J. Phys. Chem. B, Vol. 111, No. 7, 2007 **1833**

interface between polar and nonpolar media. Importantly, the simulations also have provided the first 3-D atomic-level view of a holo-form specifically incorporating two FePPIX cofactors near the juncture of the hydrophilic and hydrophobic domains of the peptide and precisely how the bundle adapts to intercalate such a relatively simple cofactor. The work provides the foundation for extension to more complex cofactors designed specifically for efficient electric charge separation and exceptional nonlinear optical properties.

References and Notes

(1) Lombardi, A.; Nastri, F.; Pavone, V. *Chem. Rev.* **2001**, *101*, 3165.

(2) Cochran, F. V.; Wu, S. P.; Wang, W.; Nanda, V.; Saven, J. G.; Therien, M. J.; DeGrado, W. F. *J. Am. Chem. Soc.* **2005**, *127*, 1346.

(3) Ye, S.; Discher, B. M.; Strzalka, J.; Xu, T.; Wu, S. P.; Noy, D.; Kuzmenko, I.; Gog, T.; Therien, M. J.; Dutton, P. L.; Blasie, J. K. *Nano Lett.* **2005**, *5*, 1658.

(4) Noy, D.; Dutton, P. L. *Biochemistry* **2006**, *45*, 2103.

(5) Xu, T.; Wu, S. P.; Miloradovic, I.; Therien, M. J.; Blasie, J. K. *Nano Lett.* **2006**, *6*, 2387.

(6) Robertson, D. E.; Farid, R. S.; Moser, C. C.; Urbauer, J. L.; Mulholland, S. E.; Pidikiti, R.; Lear, J. D.; Wand, A. J.; Degrado, W. F.; Dutton, P. L. *Nature* **1994**, *368*, 425.

(7) Dalton, L. R.; Steier, W. H.; Robinson, B. H.; Zhang, C.; Ren, A.; Garner, S.; Chen, A. T.; Londergan, T.; Irwin, L.; Carlson, B.; Fifield, L.; Phelan, G.; Kincaid, C.; Amend, J.; Jen, A. *J. Mater. Chem.* **1999**, *9*, 1905.

(8) Ye, S.; Strzalka, J. W.; Discher, B. M.; Noy, D.; Zheng, S.; Dutton, P. L.; Blasie, J. K. *Langmuir* **2004**, *20*, 5897.

(9) Strzalka, J.; Xu, T.; Tronin, A.; Wu, S. P.; Miloradovic, I.; Kuzmenko, I.; Gog, T.; Therien, M. J.; Blasie, J. K. *Nano Lett.* **2006**, *6*, 2395.

(10) Strzalka, J.; Chen, X. X.; Moser, C. C.; Dutton, P. L.; Bean, J. C.; Blasie, J. K. *Langmuir* **2001**, *17*, 1193.

(11) Churbanova, I. Y.; Tronin, A.; Strzalka, J.; Gog, T.; Kuzmenko, I.; Johansson, J. S.; Blasie, J. K. *Biophys. J.* **2006**, *90*, 3255.

(12) Huang, S. S.; Gibney, B. R.; Stayrook, S. E.; Dutton, P. L.; Lewis, M. *J. Mol. Biol.* **2003**, *326*, 1219.

(13) Skalicky, J. J.; Gibney, B. R.; Rabanal, F.; Urbauer, R. J. B.; Dutton, P. L.; Wand, A. J. *J. Am. Chem. Soc.* **1999**, *121*, 4941.

(14) Chen, X. X.; Moser, C. C.; Pilloud, D. L.; Dutton, P. L. *J. Phys. Chem. B* **1998**, *102*, 6425.

(15) Alonso, D. O. V.; Daggett, V. *Protein Sci.* **1998**, *7*, 860.

(16) Dodson, G.; Verma, C. S. *Cell. Mol. Life Sci.* **2006**, *63*, 207.

(17) Feller, S. E. *Curr. Opin. Colloid Interface Sci.* **2000**, *5*, 217.

(18) Scott, H. L. *Curr. Opin. Struct. Biol.* **2002**, *12*, 495.

(19) Ash, W. L.; Zlomislic, M. R.; Oloo, E. O.; Tieleman, D. P. *Biochim. Biophys. Acta* **2004**, *1666*, 158.

(20) Gumbart, J.; Wang, Y.; Aksimentiev, A.; Tajkhorshid, E.; Schulten, K. *Curr. Opin. Struct. Biol.* **2005**, *15*, 423.

(21) MD simulation results indicate that the rmsd of the backbone atoms of the equilibrated structure compared to that of the crystal structure is 0.80 ± 0.09 Å. The average interhelix separation is ~10.8 Å from the simulation result compared to ~10.7 Å from the crystal structure.

(22) Discher, B. M.; Noy, D.; Strzalka, J.; Ye, S. X.; Moser, C. C.; Lear, J. D.; Blasie, J. K.; Dutton, P. L. *Biochemistry* **2005**, *44*, 12329.

(23) Tikhonov, A. M.; Schlossman, M. L. *J. Phys. Chem. B* **2003**, *107*, 3344.

(24) Kono, H.; Saven, J. G. *J. Mol. Biol.* **2001**, *306*, 607.

(25) Sharp, R. E.; Diers, J. R.; Bocian, D. F.; Dutton, P. L. *J. Am. Chem. Soc.* **1998**, *120*, 7103.

(26) Zhong, Q. F.; Jiang, Q.; Moore, P. B.; Newns, D. M.; Klein, M. L. *Biophys. J.* **1998**, *74*, 3.

(27) Kale, L.; Skeel, R.; Bhandarkar, M.; Brunner, R.; Gursoy, A.; Krawetz, N.; Phillips, J.; Shinozaki, A.; Varadarajan, K.; Schulten, K. *J. Comput. Phys.* **1999**, *151*, 283.

(28) MacKerell, A. D.; Bashford, D.; Bellott, M.; Dunbrack, R. L.; Evanseck, J. D.; Field, M. J.; Fischer, S.; Gao, J.; Guo, H.; Ha, S.; Joseph-McCarthy, D.; Kuchnir, L.; Kuczera, K.; Lau, F. T. K.; Mattos, C.; Michnick, S.; Ngo, T.; Nguyen, D. T.; Prodhom, B.; Reiher, W. E.; Roux, B.; Schlenkrich, M.; Smith, J. C.; Stote, R.; Straub, J.; Watanabe, M.; Wiorkiewicz-Kuczera, J.; Yin, D.; Karplus, M. *J. Phys. Chem. B* **1998**, *102*, 3586.

(29) Jorgensen, W. L.; Chandrasekhar, J.; Madura, J. D.; Impey, R. W.; Klein, M. L. *J. Chem. Phys.* **1983**, *79*, 926.

(30) Autenrieth, F.; Tajkhorshid, E.; Baudry, J.; Luthey-Schulten, Z. *J. Comput. Chem.* **2004**, *25*, 1613.

(31) Zhang, Y. H.; Feller, S. E.; Brooks, B. R.; Pastor, R. W. *J. Chem. Phys.* **1995**, *103*, 10252.

(32) Darden, T.; York, D.; Pedersen, L. *J. Chem. Phys.* **1993**, *98*, 10089.

(33) Ryckaert, J. P.; Ciccotti, G.; Berendsen, H. J. C. *J. Comput. Phys.* **1977**, *23*, 327.

(34) Crick, F. H. C. *Acta Crystallogr.* **1953**, *6*, 689.

(35) The concept of crossing angle was borrowed from ref 31. For an idealized model of two short sections of α-helix, it is defined as the angle between the axes of the two helices. Our definition of crossing angles is the angle between the principal axes (i.e., using the coordinate axis of the principal moment of inertia) of two neighboring helices. This definition is an approximation, and it could be too coarse to be meaningful for coiled coils with several turns of the major helix or for substantially distorted helices such as the case for holo-AP0. However, first, the bundles in our case are short (around one-third of the pitch of the major helix), so the assumption that the long principal axis of the helix is approximately the axis of the helix is acceptable. Second, our calculation of the crossing angle for the helices of holo-AP0 is only for comparison with that of the apo-form and to thereby show that the holo-form is not a coiled coil.

(36) Tronin, A.; Xu, T.; Blasie, J. K. *Langmuir* **2005**, *21*, 7760.

(37) Strzalka, J.; Chen, X. X.; Moser, C. C.; Dutton, P. L.; Ocko, B. M.; Blasie, J. K. *Langmuir* **2000**, *16*, 10404.

(38) Strzalka, J.; Gibney, B. R.; Satija, S.; Blasie, J. K. *Phys. Rev. E* **2004**, *70*, 061905.